



A Neural Network Model of Chemotaxis Predicts Functions of Synaptic Connections in the Nematode *Caenorhabditis elegans*

NATHAN A. DUNN AND SHAWN R. LOCKERY*

Institute of Neuroscience, University of Oregon, Eugene, OR 97403, USA

ndunn@cs.uoregon.edu

shawn@lox.uoregon.edu

JONATHAN T. PIERCE-SHIMOMURA

Ernest Gallo Research Center Suite 200, University of California San Francisco, Emeryville, CA 94608, USA

jonp@egcrc.net

JOHN S. CONERY

Department of Computer Science, University of Oregon, Eugene, OR 97403, USA

conery@cs.uoregon.edu

Received September 8, 2003; Revised February 6, 2004; Accepted April 15, 2004

Action Editor: Karen Sigvardt

Abstract. The anatomical connectivity of the nervous system of the nematode *Caenorhabditis elegans* has been almost completely described, but determination of the neurophysiological basis of behavior in this system is just beginning. Here we used an optimization algorithm to search for patterns of connectivity sufficient to compute the sensorimotor transformation underlying *C. elegans* chemotaxis, a simple form of spatial orientation behavior in which turning probability is modulated by the rate of change of chemical concentration. Optimization produced differentiator networks capable of simulating chemotaxis. A surprising feature of these networks was inhibitory feedback connections on all neurons. Further analysis showed that feedback regulates the latency between sensory input and behavior. Common patterns of connectivity between the model and biological networks suggest new functions for previously identified connections in the *C. elegans* nervous system.

Keywords: chemotaxis, *Caenorhabditis elegans*, spatial orientation, recurrent neural networks, sensorimotor integration

1. Introduction

The complete description of the morphology and synaptic connectivity of all 302 neurons in the nematode *Caenorhabditis elegans* (White et al., 1986) raised

the prospect of the first comprehensive understanding of the neuronal basis of an animal's entire behavioral repertoire. The advent of new electrophysiological and functional imaging techniques for *C. elegans* neurons (Lockery and Goodman, 1998; Kerr et al., 2000) has made this project more realistic. Further progress would be accelerated, however, by understanding

*To whom correspondence should be addressed.

how the sensorimotor transformations underlying *C. elegans* chemotaxis could be implemented with *C. elegans*-like neuronal elements.

In previous work, we and others have identified the main features of the sensorimotor transformation underlying *C. elegans* chemotaxis (Dusenbery, 1980; Pierce-Shimomura et al., 1999), one of the two forms of spatial orientation identified in this species (Riddle et al., 1997). Locomotion during chemotaxis consists of periods of sinusoidal forward movement, called “runs,” which are punctuated by bouts of turning (occurring approximately twice a minute) (Rutherford and Croll, 1979) that have been termed “pirouettes” (Pierce-Shimomura et al., 1999). Pirouette probability is modulated by the rate of change of chemical attractant concentration ($dC(t)/dt$). When $dC(t)/dt < 0$, pirouette probability is increased whereas when $dC(t)/dt > 0$, pirouette probability is decreased. Thus, runs down the gradient are truncated and runs up the gradient are extended, resulting in net movement toward the gradient peak.

The process of identifying the neurons that compute this sensorimotor transformation is just beginning. The chemosensory neurons responsible for the input representation are known (Bargmann and Horvitz, 1991), as are the premotor interneurons for turning behavior (Chalfie et al., 1985). Much less is known about the interneurons that link chemosensory input to behavioral output (Tsalik and Hobert, 2003). To gain insight into how this transformation might be computed at the network level we used an unbiased parameter optimization algorithm to construct model neural networks capable of computing the transformation using *C. elegans*-like neurons. We found that networks with one or two interneurons were sufficient to produce this transformation. A common but unexpected feature of all networks was inhibitory feedback among all neurons. We propose that the main function of this feedback is to regulate the latency between sensory input and behavior.

2. Methods

2.1. Assumptions

We used simulated annealing (Press et al., 1992) to search for patterns of connectivity sufficient to compute the chemotaxis sensorimotor transformation. The model was constrained by three main assumptions:

1. Chemosensory neurons in *C. elegans* report attractant concentration at a single point in space.
2. Chemosensory interneurons converge on a network of locomotory command neurons to regulate turning probability.
3. The sensorimotor transformation in *C. elegans* is computed mainly at the network level, not at the cellular level.

Assumption 1 follows from the anatomy and distribution of chemosensory organs in *C. elegans* (Ward, 1973; Ward et al., 1975; Bargmann and Horvitz, 1991). Assumption 2 follows from anatomical reconstructions of the *C. elegans* nervous system (White et al., 1986), together with the fact that laser ablation studies have identified four pairs of pre-motor interneurons that are necessary for turning in *C. elegans* (Chalfie et al., 1985). Assumption 3 is heuristic.

2.2. Network

Neurons were modeled as passive, isopotential nodes according to the equation:

$$\begin{aligned} \tau_i \frac{dA_i(t)}{dt} &= -A_i(t) + \sigma(I_i) \\ I_i &= \sum_j (w_{ji} A_j(t)) + b_i \end{aligned} \quad (1)$$

where A_i is the activation level of neuron i in the network, I_i is the sum of all inputs (synaptic and/or otherwise) to neuron i , $\sigma(I_i)$ is the sigmoidal logistic function $1/(1 + \exp(-I_i))$, w_{ji} is the synaptic input from neuron j to neuron i , and b_i is static bias. The time constant τ_i determines how rapidly the activation approaches its steady-state value for constant I_i .

In conceptual terms, Eq. (1) represents a neuron whose inputs combine by simple linear addition to set the steady-state activation level. Here, however, steady-state activation is a nonlinear function of net input by virtue of the function σ . This function provides an idealized and compact representation of a variety of saturating nonlinearities that are likely to be present in real *C. elegans* neurons. Chief among these are a regenerative current that has been identified in *C. elegans* chemosensory neurons (Goodman et al., 1998), and a sigmoidal relationship between presynaptic voltage and transmitter release that has been observed in electrophysiological recordings from *Ascaris*, another species of nematode which is likely to have similar

physiology (Davis and Stretton, 1989a, 1989b). Although synaptic functions have not yet been measured electrophysiologically in *C. elegans* neurons, it is likely that *C. elegans* neurons are similar to *Ascaris* neurons in this respect, because neither species appears to signal by classical spiking neurotransmitter release.

The model of the chemosensory network had one input neuron, eight interneurons, and one output neuron (Fig. 1). The input neuron ($i = 0$) was a lumped representation of all the chemosensory neurons in the real animal. Sensory input to the network was based on the time course of attractant concentration experienced by a real worm in an actual chemotaxis assay (Pierce-Shimomura et al., 1999). The relationship between attractant concentration and sensory input current in *C. elegans* chemosensory neurons is not yet known; for simplicity we assumed a linear relationship. Accordingly, attractant concentration in the model ($C(t)$) was scaled and shifted into the range 0 to 1 and simply added to the sensory neuron's net input ($I_{i=0}$ in Eq. (1)). This convention assumes that increases in concentration depolarize the chemosensory neurons in *C. elegans*. However, we also obtained solutions under the opposite assumption (hyperpolarization). The

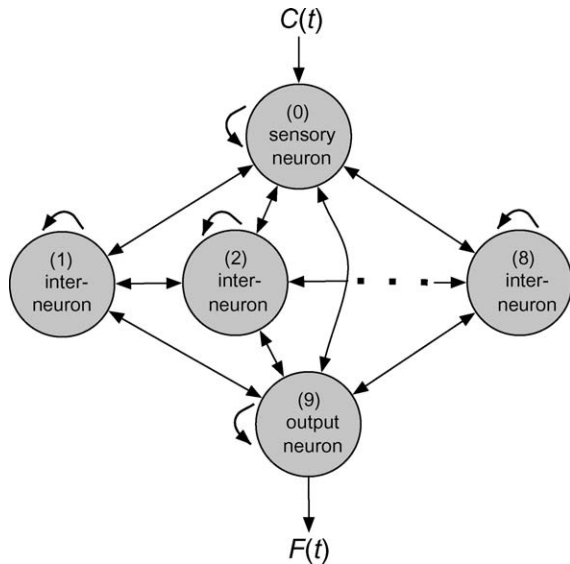


Figure 1. Model chemosensory network. Model neurons were passive, isopotential nodes. The network contained one sensory neuron, one output neuron, and eight interneurons. Input to the sensory neuron was the time course of chemoattractant concentration $C(t)$. The activation of the output neuron was mapped to turning probability by the function $F(t)$ given in Eq. (2). The network was fully connected and self-connections were allowed. Numerals indicate the index numbers by which neurons were identified.

interneurons in the model ($1 \leq i \leq 8$) represented all the chemosensory interneurons in the real animal. The output neuron ($i = 9$) abstractly represented the set of four command neurons that regulate turning behavior: AVA, AVB, AVD, and PVC (Chalfie et al., 1985; Zheng et al., 1999). The activity level of the output neuron ($A_9(t)$) determined the behavioral state of the model, i.e. its turning probability P according to the piecewise function:

$$F(t) = \begin{cases} P_{\text{high}} & A_9(t) \leq \alpha_1 \\ P_{\text{rest}} & \alpha_1 < A_9(t) < \alpha_2 \\ P_{\text{low}} & A_9(t) \geq \alpha_2 \end{cases} \quad (2)$$

where α_1 and α_2 are arbitrary thresholds determined during optimization as described in Section 2.3. We chose a piecewise function because a previous statistical analysis of intervals between turns in real worms. Figure 5(b) in Pierce-Shimomura et al. (1999) indicated the existence of distinct turning probability states.

2.3. Optimization

We optimized the chemosensory network to compute an idealized version of the true sensorimotor transformation linking $C(t)$ to turning probability (Pierce-Shimomura et al., 1999). Figure 2 shows

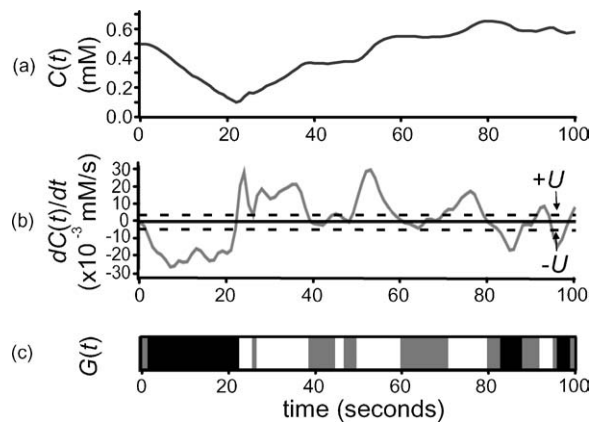


Figure 2. Construction of the idealized sensorimotor transformation used during network optimization. (a) The time course of concentration for a real worm during chemotaxis in a radial gradient of the attractant NH_4Cl . (b) The derivative of the concentration time course. (c) Desired turning probability P as a function of time. Black indicates P_{high} , grey indicates P_{rest} , and white indicates P_{low} . Desired turning probability was determined by applying Eq. (3) to the trace in (b) after being run through a low-pass filter. Thresholds ($\pm U$) are indicated by dashed lines.

how the idealized transformation was constructed. First, we computed the instantaneous derivative of the concentration time course ($C(t)$, Fig. 2(a)) recorded from a real worm during chemotaxis by subtracting neighboring points in the time course ($dC(t)/dt$, Fig. 2(b)). The subtraction procedure increased the noise due to experimental error in the original $C(t)$ trace (by additivity of variances between neighboring points). The obvious way to remove added noise is to low-pass filter the $dC(t)/dt$ trace at a corner frequency that is consistent with the time scale of chemosensory processing in *C. elegans*. To find the optimum corner frequency, we plotted the cross-correlation between the time course of pirouette-initiation probability and the sign of the low-pass filtered $dC(t)/dt$ time course over a range of corner frequencies (0.055–6.05 Hz). The cross-correlation reached a maximum at 1.35 Hz. This value was used for the results presented below. However, the main results of this paper (Table 1) were insensitive to corner frequency over the range we examined. It was reasonable to identify the optimum corner frequency via the correlation between pirouettes and the sign of $dC(t)/dt$ because previous work has shown this correlation to be the basis of *C. elegans* chemotaxis (Pierce-Shimomura et al., 1999).

We then mapped $dC(t)/dt$ to desired turning probability $G(t)$ according to the relationship:

$$G(t) = \begin{cases} P_{\text{high}} & dC(t)/dt \leq -U \\ P_{\text{rest}} & -U < dC(t)/dt < +U \\ P_{\text{low}} & dC(t)/dt \geq +U \end{cases} \quad (3)$$

where U is a threshold derived from previous behavioral observations (Fig. 7(b) in Pierce-Shimomura et al. (1999)). The result is shown in Fig. 2(c). The goal of optimization was to make the network's turning probability $F(t)$ equal to the desired turning probability $G(t)$

at all t . This was done by minimizing the average network error per time point, given by:

$$E_{\text{avg}} = \frac{1}{T} \int_0^T E(t) dt \quad (4)$$

with T equal to the number of time steps in the simulation and $E(t)$ given by:

$$\begin{aligned} \text{Case 1: } & \left. \begin{aligned} F(t) &= P_{\text{high}} \wedge G(t) = P_{\text{low}} \vee \\ F(t) &= P_{\text{low}} \wedge G(t) = P_{\text{high}} \end{aligned} \right\} E(t) = 1 \\ \text{Case 2: } & \left. \begin{aligned} F(t) &= P_{\text{high}} \wedge G(t) = P_{\text{rest}} \vee \\ F(t) &= P_{\text{rest}} \wedge G(t) = P_{\text{high}} \end{aligned} \right\} E(t) = 1/h \quad (5) \\ \text{Case 3: } & \left. \begin{aligned} F(t) &= P_{\text{low}} \wedge G(t) = P_{\text{rest}} \vee \\ F(t) &= P_{\text{rest}} \wedge G(t) = P_{\text{low}} \end{aligned} \right\} E(t) = 1/h \\ \text{Case 4: } & F(t) = G(t) \quad E(t) = 0 \end{aligned}$$

where $h \geq 1$. We introduced the parameter h simply to improve optimization efficiency. This parameter allowed us to penalize networks less for smaller deviations from the desired output (cases 2 and 3) than for larger deviations (case 1). In pilot studies with $h = 2$ we found that 87% of optimization runs converged to a solution, whereas with $h = 1$ only 14% of runs converged. Setting $h = 1$ had no effect on the main results of the paper (Table 1).

Optimization of the network was carried out by annealing three parameter types from Eq. (1): weights, time constants, and biases. Optimized networks were fully connected and self-connections were allowed. In pilot runs of the optimization algorithm, we noted that many candidate networks performed poorly (high E_{avg}) despite the fact that the activity of the output neuron ($A_o(t)$) rose and fell correctly (i.e. in anti-phase) with respect to $dC(t)/dt$. Further analysis revealed that the output neuron of the poorly performing network often had an incorrect offset, low gain, or both. To circumvent these problems, we added to the performance evaluation routine the ability to minimize E_{avg} by adjusting the thresholds α_1 and α_2 (Eq. (2)). This more generous assessment of network performance increased the efficiency of the optimization routine by an order of magnitude.

We ran the optimization algorithm 50 times on $C(t)$ data from 10 different real worms for a total of 500 networks. Although each of the 10 worms demonstrated exemplary chemotaxis (in that in that it went directly to the peak of the gradient and stayed there

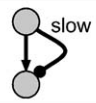


Feature	Figure	Function
direct excitatory delayed inhibitory	 slow	differentiation
self-connection		hypothesis: regulation of response latency
inhibitory recurrent connection		

Table 1. Common features of single-interneuron networks.

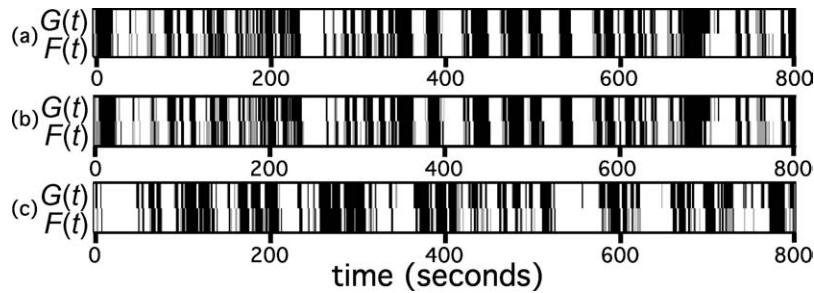


Figure 3. Network performance after optimization. In each panel ((a)–(c)), the upper trace represents $G(t)$, the desired turning probability in response to a particular $C(t)$ time course (not shown), whereas the lower trace represents $F(t)$, the resulting network turning probability. Shading signifies turning probability (black = P_{high} , grey = P_{rest} , white = P_{low}). (a) Performance of a typical network after optimization. (b) Performance of the same network after pruning to eliminate inactive interneurons. (c) Performance of the pruned network when stimulated by a different $C(t)$ time course. Note that in (a)–(c), network turning probability is delayed relative to desired turning probability because of the time required for sensory input to affect behavioral state in the model.

for the remainder of the assay), their $C(t)$ time courses were unique, ensuring a wide range of individual behavior. The result of one optimization run on one worm is illustrated in Fig. 3(a), which shows good agreement between network ($F(t)$) and desired turning probabilities ($G(t)$). We noted that in most networks many interneurons had a constant offset and showed little or no response to changes in sensory input. These interneurons were eliminated using a pruning procedure in which the tonic effect of the offset was absorbed into the bias term of postsynaptic neurons. In general, pruning had little or no effect on network performance (Fig. 3(a) versus Fig. 3(b)), suggesting that the eliminated neurons were indeed nonfunctional. Even after pruning, most of the 500 networks performed well as judged by eye. For example, 449 of the 500 networks (90%) performed at least as well as the network shown in Fig. 3(b). This result indicates that the optimization algorithm was an efficient means of finding networks capable of reproducing the chemotaxis sensorimotor transformation.

Of the 449 top-performing networks, 234 (52%) had one interneuron, 170 (38%) had two interneurons, and the remainder had three or four interneurons. We conclude that computation of the chemotaxis sensorimotor transformation does not require a large number of interneurons. For the remainder of this study, we focused on the single-interneuron networks because this was the largest class of networks.

2.4. Generalization

A key test of an optimized network is whether it responds correctly to inputs that were not presented dur-

ing optimization. We measured generalization using two independent methods.

In the first method, we challenged each of the 449 top-performing networks with $C(t)$ data from a new worm, i.e. one that was not a member of the set of 10 worms used during optimization. The $G(t)$ function (Eq. (3)) for this worm is shown in the top panel of Fig. 3(c). There was generally good agreement between network output and desired turning probability as judged by eye. We used Eq. (5) to quantify the degree of agreement, and ranked networks accordingly; 80% of the networks generalized at least as well as the network whose output $F(t)$ is shown in the lower panel of Fig. 3(c).

In the second method, we asked whether the network was able to direct locomotion of a model worm to the center of a virtual gradient. The virtual gradient was identical in shape to the real gradient that was used in actual behavioral assays (Pierce-Shimomura et al., 1999). A worm was represented as a point whose position was updated at one second intervals. Point displacement was computed from the instantaneous speed (v) and head angle (θ). Like real worms, the model worm could exist in two states: running or turning. At the beginning of each interval, the behavioral state was updated according to the current turning probability (Eq. (2)), where $P_{\text{high}} = 0.42$ and $P_{\text{low}} = 0.04$. The values for P_{high} and P_{low} were taken from fits to the exponential distributions of intervals between turns in the original statistical analysis (Pierce-Shimomura et al., 1999) (Fig. 5(b)). The value for P_{rest} (0.08) was taken from the average turning rate of real worms in the absence of a chemical gradient. Instantaneous speed was 0.15 mm/sec during runs and 0.1

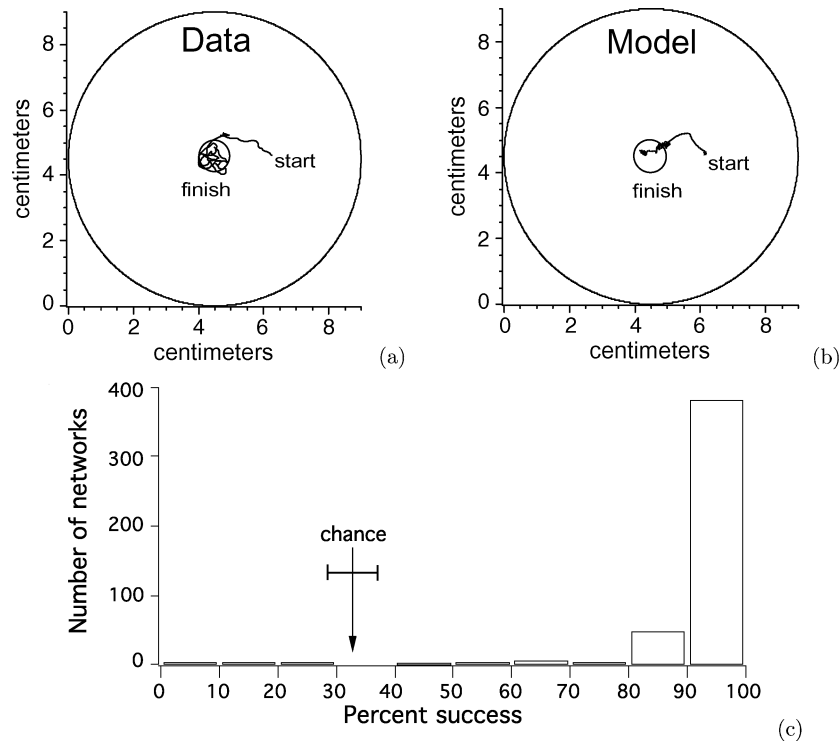


Figure 4. Test of generalization in a radial gradient. (a) Track of a real worm. (b) Track of a model worm in a virtual gradient. (c) Distribution of success rates for single neuron networks ($N = 382$). Success rate for each network was computed as the number of times a model worm reached the gradient peak (circle in (b)) in 1000 trials. The arrow indicates the average success rate ($32.4\% \pm 5\%$, 99.9% confidence interval, 200,000 trials) for a model worm in which turning probability was fixed at P_{rest} .

mm/sec during turns (Pierce-Shimomura et al., 1999). Direction was updated as follows. If the worm was in the run state, the simulation sampled from a uniform distribution of $\Delta\theta$ values where $\Delta\theta < \pm 5^\circ$. If the worm was in the turn state, the simulation sampled from a uniform distribution where $\Delta\theta > \pm 50^\circ$. Like real worms, the model worms were assayed for 1200 seconds.

As with real worms (Fig. 4(a)), most networks were able to direct the locomotion of a model worm up a virtual gradient (Fig. 4(b)). We quantified the performance of each of the 449 well-trained networks by computing its success rate in reaching the near-vicinity of the gradient's peak (circle in Fig. 4(b)) in 1000 attempts (Fig. 4(c)). 98% of the networks performed above the chance level, defined as the success rate for a model worm in which turning probability was fixed at P_{rest} . We conclude that the optimized networks showed an acceptable level of generalization in response to novel inputs.

3. Results

3.1. Common Features of Networks

All single-interneuron networks, regardless of which worm the $C(t)$ data came from, had three common features, summarized in Table 1 and Fig. 5. First, the direct pathway from sensory neuron to the output neuron was excitatory, whereas the parallel, indirect pathway via the interneuron was inhibitory. Such a circuit computes an approximate derivative of its input by subtracting a delayed version of the input from its present value (Munro et al., 1994). Second, all neurons had significant inhibitory self-connections. We noted that inhibitory self-connections were strongest on the input and output neurons, the two neurons comprising the direct pathway representing current sensory input. We hypothesized that the function of larger inhibitory self-connections was to decrease response latency in the direct pathway, perhaps by reducing the effective time

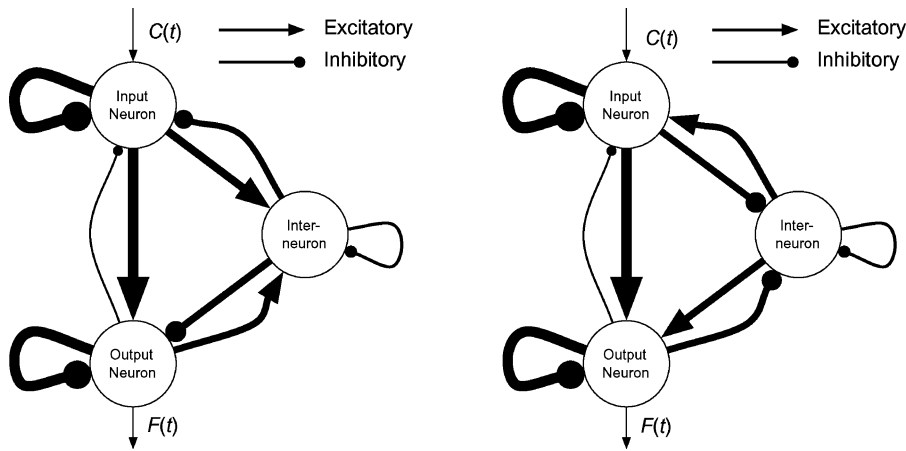


Figure 5. The two connectivity patterns observed for single-interneuron networks. Connection strength is proportional to arrow thickness. The two networks differ only in the polarity of connections to and from the interneuron, which are reversed. They are functionally equivalent because in both networks the net effect of the disynaptic pathway from input to output is inhibitory.

constant of these neurons. Such a decrease would be a means of compensating for the fact that $G(t)$ was an instantaneous function of $C(t)$, whereas the neuronal time constant τ_i tends to introduce a delay between $C(t)$ and the network's output $F(t)$. Third, the net effect of all disynaptic recurrent connections was also inhibitory. By analogy to inhibitory self-connections, we hypothesized that the function of the recurrent pathways was also to regulate response latency.

3.2. Output Delay

To test the hypothetical functions of the self-connections and recurrent connections, we introduced an explicit time delay (Δt) between $dC(t)/dt$ and the desired turning probability $G(t)$ such that:

$$G'(t) = G(t - \Delta t) \quad (6)$$

$G'(t)$ was substituted for $G(t)$ during optimization. We then repeated the optimization procedure with a range of Δt values (0 to 3 seconds) and looked for systematic effects on weights and time-constants (Fig. 6).

Effects on Self-Connections. We found that the strengths of self-connections on all three neurons were inversely related to Δt (Fig. 6(a), ANOVA: input neuron $F_{3,309} = 51.98$, $p < 0.001$; interneuron $F_{3,309} = 9.441$, $p < 0.001$; output neuron $F_{3,309} = 63.54$, $p < 0.001$). This result is consistent with the hypothesis that

the function of these self-connections is to regulate response latency.

Effects on Recurrent Connections. We quantified the strengths of recurrent connections by taking the products of the two weights along each of the three recurrent loops in the network. We found that the strengths of the two recurrent loops that included the interneuron were inversely related to Δt (Fig. 6(b), ANOVA: input neuron to interneuron $F_{3,309} = 4.14$, $p < 0.005$; output neuron to interneuron $F_{3,309} = 2.755$, $p < 0.05$). This result suggests that the function of these loops is to regulate response latency and supports the hypothetical function of the recurrent connections. Interestingly, however, the strength of the recurrent loop between input and output neurons was not affected by changes in Δt ($F_{3,309} = 1.361$, $p = 0.255$). Thus, effects on recurrent loop products were limited to two of the three loops in the network.

Effects on Time Constants. We found that the time constants of the input neuron and the output neuron increased with output delay (Fig. 6(c), ANOVA: input neuron $F_{3,309} = 19.9$, $p < 0.001$; output neuron $F_{3,309} = 21.56$, $p < 0.001$). This result suggests that time constants also contributed to the regulation of response latency. However, we noted that there was no effect of training delay on the time constant of the interneuron ($F_{3,309} = 1.791$, $p = 0.149$). Thus, effects on time constants were restricted to two of the three neurons in the network.

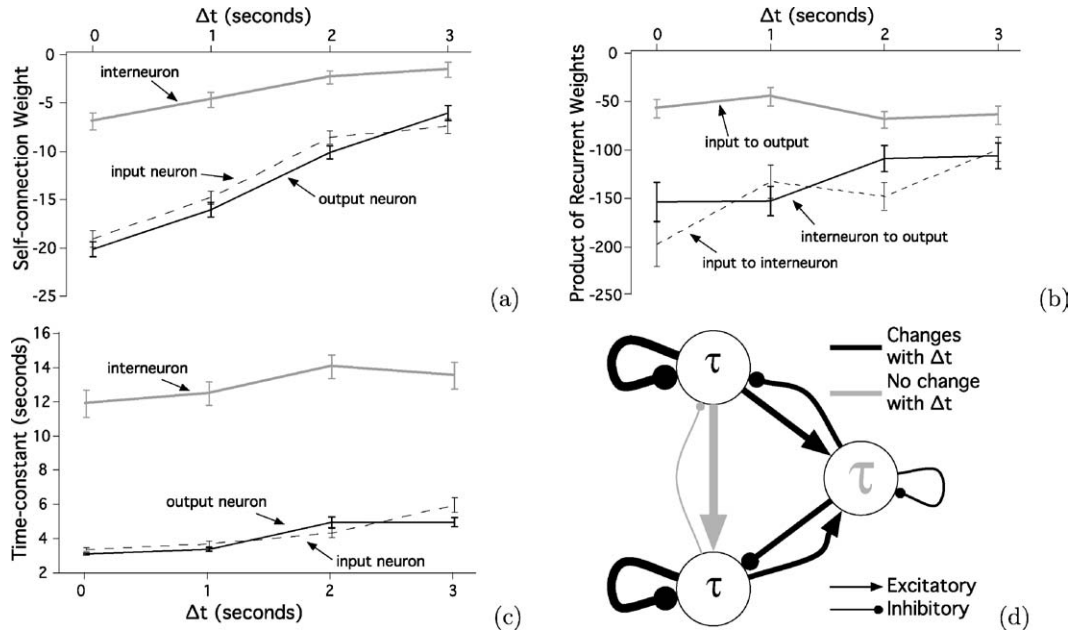


Figure 6. The effect of output delay (Δt) on network parameters. Plotted points are averages with error bars representing standard error. (a) Self-connections. (b) Recurrent connections. Recurrent connection strength was quantified by taking the product of the weights along each of the three recurrent loops in Fig. 5. (c) Time constants. (d) Summary of effects. Parameters affected by changes in output delay are shown in black. Unaffected parameters are shown in grey. The average time constant is proportional to the font-size of τ shown in the neuron. Average connection magnitude is proportional to line width. Parameter magnitudes are shown only for $\Delta t = 0$.

Figure 6(d) summarizes the effects of output delays. The changes reflect two distinct mechanisms for regulating latency. Changes in self-connections and time constants represent cellular level mechanisms, whereas changes in the strengths of recurrent connections represent network level mechanisms. The two mechanisms were distributed differently within the network. The cellular level mechanism was confined to the input and output neurons, whereas the network level mechanism was confined to synaptic pathways involving the interneuron. The difference between the distributions of the two mechanisms could reflect performance trade-offs. Alternatively, differences could also reflect properties of the optimization algorithm.

3.3. Analysis

Self-Connections. To provide a theoretical explanation for the effects of time delays on the magnitude of self-connections, we analyzed the step response of Eq. (2) for a reduced system containing a single linear neuron with a self-connection, which is given by:

$$\tau_i \frac{dA_i(t)}{dt} = w_{ii} A_i(t) - A_i(t) + h(t) \quad (7)$$

where $h(t)$ represents a generic external input (sensory or synaptic). Solving Eq. (7) for $h(t)$ equal to an instantaneous step of amplitude M at $t = 0$ with $A_i(0) = 0$ gives:

$$A_i(t) = \left(\frac{M}{1 - w_{ii}} \right) \left[1 - \exp \left[- \left(\frac{1 - w_{ii}}{\tau_i} t \right) \right] \right] \quad (8)$$

From Eq. (8), when $w_{ii} = 0$ (no self-connection) the neuron relaxes to steady-state at the rate $1/\tau_i$, whereas when $w_{ii} < 0$ (inhibitory self-connection) the neuron relaxes at the higher rate of $(1 + |w_{ii}|)/\tau_i$. Thus, single-neuron response latency drops as the strength of the inhibitory self-connection increases and, conversely, response latency rises as self-connection strength decreases. This result explains the effect on self-connection strength of introducing a delay between $dC(t)/dt$ and turning probability (Fig. 6(a)). This result is also consistent with the fact that the magnitudes of the interneuron self-connection were consistently smaller than the magnitude of the other two self-connections. Smaller interneuron self-connections lead to longer response latencies in this neuron, whose function is to present a delayed version of the input to the output neuron.

Recurrent Inhibitory Connections. We made a similar analysis of the effects of time delays on the recurrent connections. Here, however, we studied a reduced system of two linear neurons with recurrent synapses and an external input to one of the neurons.

$$\tau_i \frac{dA_i(t)}{dt} = w_{ji} A_j(t) - A_i(t) + h(t) \quad (9)$$

$$\tau_j \frac{dA_j(t)}{dt} = w_{ij} A_i(t) - A_j(t) \quad (10)$$

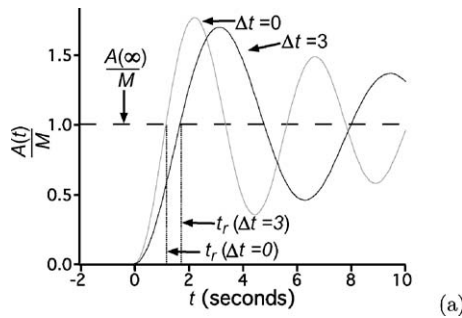
We solved this system for the case where the external input $h(t)$ is an instantaneous step of size M that occurs at time $t = 0$, with $A_i(0) = A_j(0) = 0$, and $\tau_i = \tau_j = \tau$. For the case where $w_{ij}w_{ji} < 0$, the solution to Eqs. (9) and (10) are 2nd-order differential equations with complex roots:

$$A_i(t) = 1 - \left(\frac{\sqrt{1 - w_{ij}w_{ji}}}{\sqrt{-w_{ij}w_{ji}}} \right) \exp(-t/\tau) \times \sin \left(\left(\frac{\sqrt{-w_{ij}w_{ji}}}{\tau} (1 + \sqrt{-w_{ij}w_{ji}}) \right) t + \phi \right) \quad (11)$$

$$A_j(t) = \left(\frac{Mw_{ij}}{1 - w_{ij}w_{ji}} \right) \times \left[1 - \left(\frac{\sqrt{1 - w_{ij}w_{ji}}}{\sqrt{-w_{ij}w_{ji}}} \right) \exp(-t/\tau) \sin \left(\frac{\sqrt{-w_{ij}w_{ji}}}{\tau} t + \phi \right) \right] \quad (12)$$

$$\phi = \arctan(\sqrt{-w_{ij}w_{ji}}) \quad (13)$$

The step response of the two-neuron system is an underdamped oscillation (Fig. 7(a)). The extent to which



the oscillation is damped is given by the damping coefficient:

$$\Psi = \frac{1}{\sqrt{1 - w_{ij}w_{ji}}} \quad (14)$$

Damping affects several key aspects of the step response including rise time (t_r), which is defined as the latency between step onset and the time it takes output to first cross its eventual steady-state value. From Eq. (14) it is evident that as the strength of the recurrent loop (i.e. $|w_{ij}w_{ji}|$) decreases, damping increases (Fig. 7(b)). Thus, response latency rises as the strength of the recurrent loop decreases. This result explains the effect on recurrent loop strength of introducing a delay (Δt) between $dC(t)/dt$ and turning probability (Fig. 6(b)).

4. Discussion

We used simulated annealing to search for networks capable of computing an idealized version of the chemotaxis sensorimotor transformation in *C. elegans*. We found that one class of such networks is the three-neuron differentiator with inhibitory feedback. The appearance of differentiator networks was not surprising (Munro et al., 1994) because the networks were optimized to report, in essence, the sign of $dC(t)/dt$ (Eq. (3)). The prevalence of inhibitory feedback, however, was unexpected. Inhibitory feedback was found at two levels: self-connections and recurrent connections. Combining an empirical and theoretical approach, we have argued that inhibitory feedback at both levels

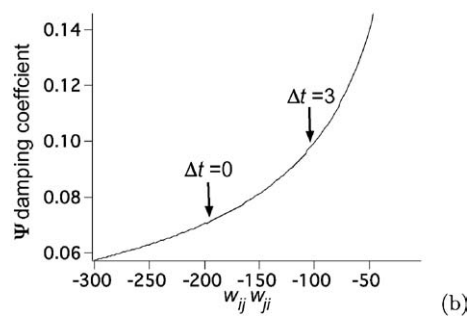


Figure 7. Analysis of two linear neurons with recurrent synapses. (a) Response of the system to an instantaneous step of magnitude M occurring at $t = 0$. The grey line shows the response $A(t)$ when the product of the recurrent connections ($w_{ij}w_{ji}$) is the average value of the input to interneuron loop obtained for networks optimized for output delay $\Delta t = 0$. The dark line shows the response when the recurrent product optimized with $\Delta t = 3$. Rise time (t_r), the time it takes $A(t)$ to first cross its eventual steady-state output, increases as Δt increases. (b) Plot of the relationship of damping coefficient to the product of weights on recurrent synapses. Arrows indicate the values of the damping coefficient for average values of the recurrent product. These averages were obtained at the indicated output delay Δt .

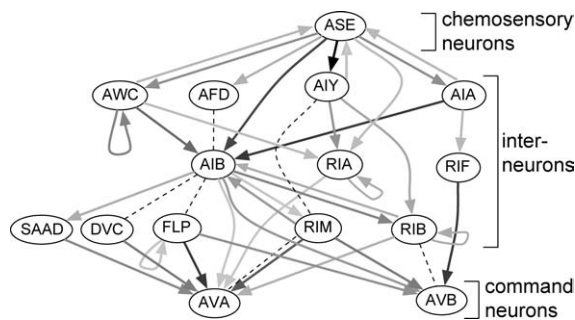


Figure 8. The network of chemosensory interneurons in *C. elegans*. Shown are the interneurons interposed between the chemosensory neuron ASE and the two locomotory command neurons AVA and AVB on the basis of their anatomical connections. These interneurons are hypothetical members of the chemotaxis network. Whether or not they actually play a role in chemotaxis remains to be tested. The diagram is restricted to interneuron pathways with at most three synapses. Arrows represent chemical synapses. Dashed lines represent gap junctions. Pathways containing synaptic partners with fewer than two presynaptic densities, or fewer than three gap junctions, were omitted. Connectivity is inferred from the anatomical reconstructions (White et al., 1986). Left and right symmetrical pairs are collapsed into single neurons and the number of connections to the pair is summed. Chemical synapses connecting symmetrical pairs are drawn as self-connections. Gap junctions connecting symmetrical pairs are not shown.

could function to regulate the response latency of the system's output relative to its input. Such regulation would be significant in the *C. elegans* nervous system if the membrane time constant were a limiting factor in response latencies.

There are intriguing parallels between our three-neuron network models and the biological network. Figure 8 shows the network of interneurons interposed between the chemosensory neuron class ASE, the main chemosensory neurons for salt chemotaxis, and the locomotory command neurons classes AVA and AVB. The interneurons in Fig. 8 are candidates for computing the sensorimotor transformation for chemotaxis in *C. elegans*. Three parallels are prominent. First, there are four candidate differentiator circuits, as noted previously (White, 1985). These circuits are formed by the neuronal triplets ASE-AIY-RIA, ASE-AIA-AIB, ASE-AFD-AIB and ASE-AWC-AIB. Second, there are self-connections on three neuron classes in the circuit, including AWC and RIA, which may both be involved in the differentiator circuits. These self-connections represent anatomically identified connections between left and right members of the respective neuron pair; we represented them here as self-connections because each member of a pair is pre- and post-synaptic to

analogous neurons and so the two neurons probably function as a single unit. It remains to be seen, however, whether these connections are inhibitory in the biological network. Self-connections could also be implemented at the cellular level by voltage dependent currents. A voltage-dependent potassium current, for example, can be functionally equivalent to an inhibitory self-connection because depolarization of the neuron recruits a hyperpolarizing current. Electrophysiological recordings from ASE and other neurons in *C. elegans* confirm the presence of such currents (Goodman et al., 1998; Nickell et al., 2002). Thus, it is conceivable that many neurons in the biological network have the cellular equivalent of self-connections. Third, there are reciprocal connections between ASE and three of its six postsynaptic targets. These connections could provide recurrent inhibition if they have the appropriate signs.

Common patterns of connectivity between the model and biological networks suggest new functionality for previously identified connections in the *C. elegans* nervous system. It should be possible to test these functions through electrophysiological recordings, calcium imaging, and neuronal ablations.

Acknowledgments

We are grateful to Don Pate for technical assistance. Supported by NSF IBN-0080068.

References

- Bargmann CI, Horvitz HR (1991) Chemosensory neurons with overlapping functions direct chemotaxis to multiple chemicals in *C. elegans*. *Neuron* 7: 729–742.
- Chalfie M, Sulston J, White J, Southgate E, Thomson J, Brenner S (1985) The neural circuit for touch sensitivity in *C. elegans*. *J. Neurosci.* 5: 956–964.
- Davis RE, Stretton AOW (1989a) Passive membrane properties of motoneurons and their role in long-distance signaling in the nematode *Ascaris*. *J. Neurosci.* 9: 403–414.
- Davis RE, Stretton AOW (1989b) Signaling properties of *Ascaris* motoneurons: Graded active response, graded synaptic transmission, and tonic transmitter release. *J. Neurosci.* 9: 415–425.
- Dusenbery D (1980) Responses of the nematode *C. elegans* to controlled chemical stimulation. *J. Comp. Physiol.* 136: 127–331.
- Goodman M, Hall D, Avery L, Lockery S (1998) Active currents regulate sensitivity and dynamic range in *C. elegans* neurons. *Neuron* 20: 763–772.
- Kerr R, Lev-Ram V, Baird G, Vincent P, Tsien RY, Schafer WR (2000) Optical imaging of calcium transients in neurons and pharyngeal muscle of *C. elegans*. *Neuron* 26: 583–594.

- Lockery SR, Goodman MB (1998) Tight-seal whole-cell patch clamping of *C. elegans* neurons. *Methods Enzymol.* 293: 201–217.
- Munro E, Shupe L, Fetz E (1994) Integration and differentiation in dynamical recurrent neural networks. *Neural Comput.* 6: 405–419.
- Nickell W, Pun R, Bargmann C, Kleene S (2002) Single ionic channels of two *C. elegans* chemosensory neurons in native membrane. *J. Membr. Biol.* 189(1): 55–66.
- Pierce-Shimomura JT, Morse TM, Lockery SR (1999) The fundamental role of pirouettes in *C. elegans* chemotaxis. *J. Neurosci.* 19: 9557–9569.
- Press W, Teukolsky S, Vetterling W, Flannery B (1992) *Numerical Recipes in C*. 2nd edn Cambridge University Press, New York.
- Riddle D, Blumenthal T, Meyer B, Priess J (eds) (1997) *C. elegans II*. Cold Spring Harbor Laboratory Press.
- Rutherford T, Croll N (1979) Wave forms of *C. elegans* in a chemical attractant and repellent and in thermal gradients. *J. Nematol.* 11: 232–240.
- Tsalik L, Hobert O (2003) Functional mapping of neurons that control locomotory behavior in *C. elegans*. *J. Neurobiol.* 56: 178–197.
- Ward S (1973) Chemotaxis by the nematode *C. elegans*: Identification of attractants and analysis of the response by use of mutants. *Proc. Natl. Acad. Sci. USA* 70: 817–821.
- Ward S, Thomson N, White JG, Brenner S (1975) Electron microscopical reconstruction of the anterior sensory anatomy of the nematode *C. elegans*. *J. Comp. Neurol.* 160: 313–338.
- White J (1985) Neuronal connectivity in *C. elegans*. *Trends Neurosci.* 8: 277–283.
- White JG, Southgate E, Thomson JN, Brenner S (1986) The structure of the nervous system of the nematode *C. elegans*. *Philos. T. Roy. Soc. B [Biol.]* 314: 1–340.
- Zheng Y, Brockie PJ, Mellem JE, Madsen DM, Maricq AV (1999) Neuronal control of locomotion in *C. elegans* is modified by a dominant mutation in the *glr-1* ionotropic glutamate receptor. *Neuron* 24: 347–361.